

<i>Cryst. Res. Technol.</i>	35	2000	6–7	851–862
-----------------------------	----	------	-----	---------

R. A. SCHWARZER, A. HUOT

Physikalisches Institut der TU, AG Textur, Clausthal-Zellerfeld, Germany

## The Study of Microstructure on a Mesoscale by ACOM

*Dedicated to Prof. Dr. J. Heydenreich on the occasion of his 70<sup>th</sup> birthday*

The benefits of analytical electron microscopy are the correlation of morphology, elemental composition and crystal structure on a submicron scale. Automated crystal orientation measurement (ACOM) in the SEM enables, by digital beam scan, the convenient and fast acquisition of orientation data in selected bulk surface areas grain by grain. Grain boundaries exceeding some tenth of a degree of misorientation are reliably identified. The quality of backscatter Kikuchi patterns is a (semi-) quantitative measure of local plastic deformation. The database can be used for crystal orientation mapping (COM), quantitative texture analysis (ODF, pole figures, MODF), characterization of grain and phase boundaries, and orientation stereology in general from macroscopic areas down to mesoscale.

Keywords: ACOM, EBSD, crystal texture, electromigration, electron diffraction, SEM

(Received May 11, 2000; Accepted July 1, 2000)

### 1. Introduction

The great majority of natural as well as technologically used materials occur in the crystalline rather than amorphous state. They are usually polycrystals with preferred rather than randomly distributed grain orientations. In addition, they may be composed of different phases. Therefore, the following structural parameters have to be known to characterize the real microstructure of a material:

- Phase structure: Crystal structure, i.e. the positions of the atoms in the unit cells, and elemental composition of the phases.
- Stereology: Volume fractions of the phases; (statistical distributions of) size, shape and mutual arrangement of the phases and monocrystalline volume elements (i.e. the grains).
- Crystallographic texture: Macrottexture (described by the orientation density function (ODF) or pole figures) and mesoscale texture (described by the spatial arrangement of grain orientations and the characterization of grain/phase boundaries).
- Substructure: Any deviation of the grains from the ideal crystal structure, e.g., point defects, dislocations, solid solution, ordering, stacking faults and twins, lattice strain/local residual stress.

A comprehensive description of microstructure spans over a large range from the macroscopic dimensions of the end product down to the microscale of substructural defects in the grains. Therefore, a variety of sophisticated experimental techniques have to be employed for measurement. Depending on the point of view and the availability of techniques, two separate branches of traditional materials science are used which emphasize either the morphology or the crystallographic aspects of microstructure. These two technologies have developed almost without mutual interaction:

- *Stereology* or *Quantitative Metallography* is based on microscopy techniques to reveal the morphology, but with omission of the grain orientations.
- *Crystal Texture Analysis* was based until recently on pole-figure measurement by diffraction methods without considering the spatial coordinates.

Most physical properties of a polycrystalline solid depend in a complex way on all the structural parameters mentioned above. They may change along with the structural parameters during the production process and service of a product. Often they are tensorial properties,  $P(g)$ , i.e. they depend on the crystallographic orientation,  $g$ . This is evident from the anisotropy of properties of the single crystal, but an overall anisotropy,  $\overline{P(g)}$ , results also for polycrystals, unless their grains are oriented at random. Since structural and functional materials are often employed to the extreme, flaws or even small local variations of property may cause a failure. Tabulated characteristic property values averaged over large sample volumes or all crystal orientations should hence be considered as semi-quantitative predictors of the materials behavior only.

Advanced materials demand for a more general description of microstructure which considers at the same time the distributions of size, shape, arrangement, orientation and defects of the constituent grains and phases in three-dimensional real space. For this purpose the *microstructure function* [BUNGE and SCHWARZER, 2000] (also named *aggregate function* [BUNGE, 2000])

$$G(r) = \begin{cases} i(r) & \text{phases} \\ g(r) & \text{orientations} \\ S(r) & \text{defects, local lattice strain} \end{cases}$$

has been introduced.  $i = \{i_1, i_2, \dots, i_n\}$  denotes the phases which are characterized by their crystal structure and elemental composition,  $g = \{\mathbf{j}_1, \mathbf{F}, \mathbf{j}_2\}$  are the orientation parameters, and  $S = \{s_1, s_2, \dots, s_n\}$  are the substructure parameters. They are specified in volume elements at the places  $r = \{x, y, z\}$ . Without considering the grain substructure, the microstructure function of each phase  $G^i(r)$  depends already on three spatial,  $\{x, y, z\}$ , and three orientation coordinates,  $\{\mathbf{j}_1, \mathbf{F}, \mathbf{j}_2\}$ , in a six-dimensional hyperspace that is almost beyond human imagination. Conventional stereological parameters, for instance volume fractions of the phases or grain size distributions, are treated in close relation with crystal texture, such as the orientation density function (ODF), pole figures, texture fields  $f(x, g)$ , the misorientation distribution function (MODF) and orientation correlation functions, phase and grain boundaries, and orientation-dependent property fields  $\overline{P(x)} = \int P(g) \cdot f(x, g) dg$ .

## 2. Experimental Determination of the Microstructure Function

The structural parameters are not equally easy to measure. A phase is defined primarily by its crystal structure and the resulting materials properties rather than its elemental composition. Phases in larger specimen volumes are commonly determined by interpreting the positions and intensities of peaks in x-ray diffraction spectra. However, specific experimental difficulties arise with multi-phase materials due to a large number of diffraction peaks, peak overlap, small volume fractions, and effects of texture and anisotropic absorption on peak intensity. Microbeam electron diffraction as well as dark-field imaging using phase-specific reflections in the TEM enable best spatial resolution and still a high reliability in phase discrimination [BRÜMMER et al., 1980].

Energy dispersive x-ray spectroscopy (EDS) in the SEM is widely used as *the* standard technique for (semi-)quantitative elemental analysis and element mapping at a meso-scale.

Phase discrimination and moreover phase identification solely based on elemental analysis may fail, since in general there exists a range of miscibility of the components forming an alloy. In addition, materials used for technical applications are hardly in a state of thermal equilibrium. Allotropic transformations occur without any change in chemical composition. They go unnoticed by elemental analysis. The same objection holds true for other (imaging) microanalytical techniques like SIMS, Auger or EELS.

The stereological evaluation of microstructure images is straightforward, if the phases and/or grains show a sufficient specific image contrast in the light or scanning electron microscope. In most cases, however, an etch specific for the phases, the grain orientations or grain boundaries is required to produce a surface relief. Needless to say that the reliability of metallographic etching depends on the skill of the metallographer. It is worth mentioning here that in general neither phase contrast is specific enough for phase determination, nor enables orientation contrast the determination of grain orientations.

Since decades, pole-figure measurement by x-ray or neutron diffraction is a well-established technique in materials science for the determination of global texture as an average characteristics of microstructure over relatively large specimen areas [BUNGE, 2000]. A scanning x-ray apparatus with an energy-dispersive detector system enables the measurement of pole-figures of selected small areas as well as the simultaneous acquisition of distribution maps of texture, residual lattice strain and elements (imaging x-ray fluorescence analysis) in bulk surfaces at a special resolution of 0.1 mm or better [FISCHER and SCHWARZER, 1998].

A concept similar to the x-ray diffraction technique has been realized in the TEM to study texture of small areas in thin free-standing foils or on bulk surfaces by SAD as well as RHEED pole-figure measurement, respectively [SCHÄFER and SCHWARZER, 1998]. Individual grain orientation measurement at a high spatial resolution down to some ten nanometer is achieved in the TEM by automated interpretation of Kikuchi patterns [SCHWARZER and SUKKAU, 1998]. By simulating the effect of specimen tilt on the diffraction pattern, the on-line analysis of Burgers vectors and deformation systems is facilitated considerably.

The outstanding benefits of analytical electron microscopy [BETHGE and HEYDENREICH, 1980; REIMER, 1984] are the high spatial resolutions in imaging and diffraction which allow, on a submicron scale, the correlation of morphology (from bright and dark-field or weak beam micrographs) and elemental composition (from EDS or EELS analysis) with crystallographic structure (determination of phase and crystal lattice orientation from microbeam or SAD diffraction). Convergent beam electron diffraction is an extremely sensitive tool to study lattice distortions and to determine phases from HOLZ patterns at nanometer resolution. CBED patterns may be used on a grain-specific level either for the determination of local foil thickness and structure potentials of the crystal lattice, or for the determination of the crystal lattice symmetry (space and point group) and for phase analysis, for the characterization of stacking faults and Burgers vectors, and for residual stress measurement. They are of very limited use for crystal lattice orientation measurement. Last but not least, HRTEM enables the determination of the positions of rows of atoms in the real crystal and in particular along grain and phase boundaries, provided that the boundary plane and a low-index zone axis on each side of the boundary are standing parallel with the primary beam direction. HRTEM thus enables the ultimate description of microstructure. However, the preparation of transparent thin specimens for the TEM is tedious, impractical or almost impossible with multiphase materials, in particular if larger sample areas have to be studied. Specimen preparation may also induce unwanted artifacts or lead to relaxation effects such that thin foils are no longer representative for the bulk. The TEM is therefore, although extremely powerful in dedicated applications, often of limited use to answer questions of practical materials science.

### 3. Automated Crystal Orientation Measurement/Mapping with the SEM

A break-through in the quantitative characterization of microstructure of bulk crystalline materials has been achieved recently with the development of automated systems for backscatter Kikuchi diffraction (BKD) in the SEM [ADAMS et al., 1993]. This new technique is known as "ACOM" (Automated Crystal Orientation Measurement/Mapping) or "Automated EBSD" (Automated Electron BackScatter Diffraction). Four commercial ACOM systems are available at present that are "ChannelPlus™" from HKL Technology, "OIM™" from TexSEM Laboratories, "OPAL™" from Oxford Instruments, and "ORKID™" from Noran Instruments. Therefore, the user of an SEM need not undergo the trouble of developing an ACOM system on his own.

Backscatter Kikuchi patterns (BKP) [NISHIKAWA and KIKUCHI, 1928; ALAM et al., 1954] are formed if the stationary beam of energetic primaries impinges on a virtually perfect volume of crystal. Some portion of the primary electrons are backscattered through large angles. The increase in wavelength due to the energy loss by a scattering event, however, is negligibly small, and they can thus be considered as incoherent new beams emerging from a point source in the crystal. If they fall under Bragg's angle  $\vartheta$  on a set of parallel lattice planes with spacings  $d_{hkl}$ , they can be diffracted. Bragg's law

$$\sin \vartheta = n\lambda/2d_{hkl} \quad (1)$$

means that the incoming and the diffracted beams form a double cone about the lattice plane normal with an apex angle of  $90^\circ - \vartheta$ , named Kossel cone I and II. Since the wavelength of energetic electrons,  $\lambda$ , is small compared to interplanar spacings, the Bragg angles are in the range of a few degree or less only. Hence the conic sections I and II with a flat screen degenerate to a pair of narrow parallel straight lines, the so-called Kikuchi lines, which border the related Kikuchi band of angular width  $2\vartheta$ . Those beams which miss Bragg's condition continue penetrating through the crystal in their directions after inelastic scattering to form an intense background. Due to the wide-angle scattering in the first step, the convergence of the primary beam has virtually no effect on pattern formation. Spot size, however, has to be reduced on real polycrystals so far that interaction with matter occurs only in an almost perfect small volume of the crystallite. Otherwise Kikuchi patterns are generated from distorted volume elements which are slightly rotated against each other. They are superimposed on the screen and blur out rapidly with increasing imperfection of the substructure.

According to this simple geometrical theory, the Kikuchi pattern can be interpreted as a gnomonic projection of the crystal lattice on the flat phosphor screen: The point of impingement of the primary beam on the specimen surface is the center of projection. In particular the angles between the center lines correspond to the interplanar angles, and the spacings of line pairs correspond to the interplanar spacings according to Bragg's law. When tilting or rotating the specimen, the Kikuchi lines rigidly and precisely follow every rotary movement of the crystal. This feature is the basis for a precise lattice orientation measurement. The extinction rules due to the structure factor of the crystal lattice apply for expected reflections, and high order reflections may appear as a set of further parallel straight lines. In a real backscatter Kikuchi pattern the space between a pair of Kikuchi lines from low-index lattice planes usually shows higher intensity than the neighboring background, and a bright Kikuchi band is seen. The bands intersect in low-index zone axes that form star-like poles. Kikuchi bands rather than Kikuchi lines and poles are the most prominent features of this type of pattern. The intensity distribution of a Kikuchi pattern is not explained by the geometric model, but the dynamic theory of electron diffraction has to be employed [BRÜMMER and STEPHANIK, 1976; REIMER, 1984]. For indexation and crystal orientation

measurement, however, the geometrical features of band width and band position as mentioned above are sufficient.

Inelastic scattering of energetic electrons shows a pronounced anisotropy with a steep maximum in forward direction. In order to obtain a backscatter Kikuchi pattern of sufficient intensity, the bulk specimen has to be steeply tilted out of the horizontal plane such that the surface makes a small angle of typically  $20^\circ$  with the primary beam and no longer intercepts the pattern forming electrons. The steep specimen tilt has several unfavorable consequences: The image and the beam spot are foreshortened by about 1/3. The beam spot runs out of focus when scanning down the specimen line after line. Standard SE and BE detectors are inadequate, because the signal fades away when scanning down the surface. Long working distances must be used at the expense of high resolution and beam current, if large specimens have to be accommodated in the chamber. A steep specimen tilt is incompatible with most quantitative EDS programs which means an obstacle to simultaneous elemental analysis and crystal orientation measurement.

A backscatter Kikuchi pattern is superimposed on a background that is more than one order of magnitude higher than the useful signal. Moreover, background intensity is uneven with a steep drop from the forward scattering direction. Background depends also on the grain orientation, i.e. the actual diffraction pattern. As a consequence, background varies during wide beam scans with the spot position on the specimen surface as well as with local specimen density (phase) and surface relief. A further fluctuation of background may be caused by variations of the probe current due to instabilities of the emission current of the gun, drift in the alignment of the column, specimen charging, or built-up of carbon contamination. The automated recognition of faint Kikuchi patterns on a steep background may then become extremely difficult. Fortunately, the quality of backscatter Kikuchi patterns is improved significantly by "flat fielding": The raw pattern is normalized to a flat field image which contains the background and image artifacts (e.g., scratches on the screen, blind or bright dots on the camera chip), but no structure from the Kikuchi pattern. A flat field image can be obtained experimentally, e.g. by a scan across several grains or by defocusing the primary beam to the extreme. Alternatively, background can be reconstructed from the actual diffraction pattern by dedicated software filtering [SCHWARZER and SUKKAU, 1998].

With our ACOM system, the SEM is under full control of the external computer which comprises digital beam scan, final lens current, magnification, accelerating voltage, modes of SEM operation, operation modes of the digital signal processor (DSP) and pattern acquisition (Figure 1) [SCHWARZER, 1997a]. Switching the DSP and the SEM between imaging and spot mode is used for automated flat fielding. After a user-selected number of scanned points or when indexing has failed for a few subsequent points, a new flat field image is acquired, without the operator having to interact, for background correction. The control of the final lens current (respectively the working distance), microscope magnification and scan rotation are used for dynamic system calibration and dynamic focusing "on the fly". Since spatial resolution depends on the size of the beam spot rather than on the actual magnification, a high spatial resolution is thus enabled, irrespective of low microscope magnification. A large specimen area or distant surface regions can thus be studied by digital beam scan in a sequence without having to translate the sample. The accelerating voltage is read as a measure of electron wavelength when the band widths are optionally used for indexing. A mechanical stage scan ("OIM<sup>TM</sup>") [ADAMS et al., 1993] can do without dynamic calibration and focusing procedures, since the diffraction geometry does not change from one measured point to the next. However this alternative for digital beam scan is less precise and too slow to enable the acquisition of a sufficiently large number of grain orientations in a reasonable time. A high-precision, computer-controlled mechanical stage is furthermore a delicate and costly add-on facility to an SEM.

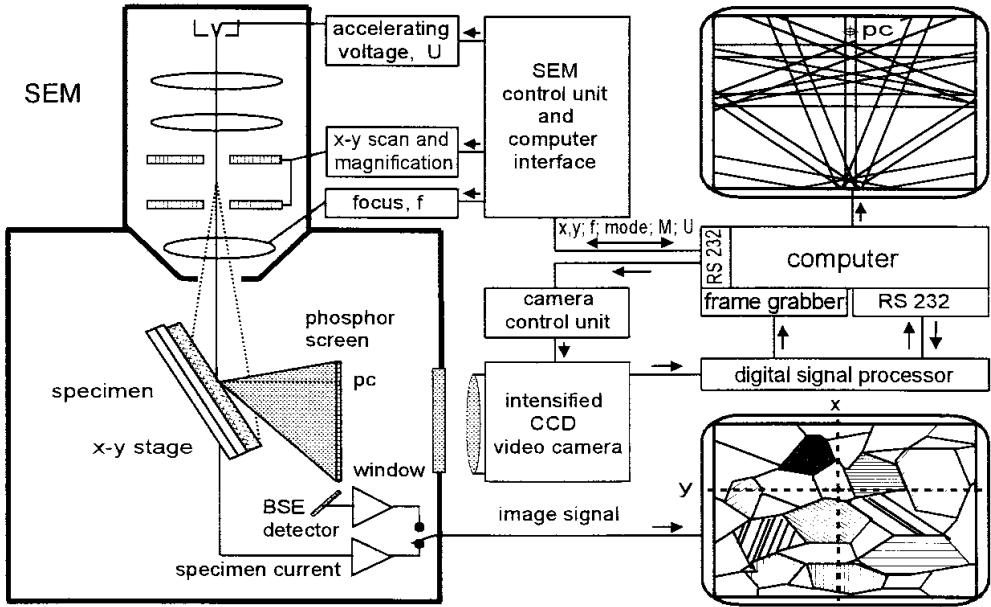


Fig. 1: Setup of an advanced ACOM system.

A fully automated EBSD system consists of the following main components: computer-controlled beam or stage scan, hardware for real-time pattern acquisition and digitization (phosphor screen, low-light level CCD camera, digital signal processor and framegrabber) (Figure 1), software for automated pattern acquisition and recognition to locate the Kikuchi bands, software for indexing Kikuchi patterns and finally software for the calculation of crystal orientations with respect to a fixed laboratory coordinate system. Details can be found elsewhere [SCHWARZER, 1997a]. A particular challenging task is the automated extraction of the positions of Kikuchi bands in a pattern, because they are often diffuse, broad stripes of non-uniformly distributed intensity on a high background rather than sharp continuous lines. The usual line filtering, gradient, or contour tracing methods are not well suited for noisy images with fragmentary motifs. We apply a *Radon transform* (RADON, 1917; DEANS, 1983) on the background-corrected patterns. The polar equation of a straight line is

$$\mathbf{r} = x \cdot \cos \mathbf{e} + y \cdot \sin \mathbf{e} \tag{2}$$

$\mathbf{r}$  stands for the distance of the line from the origin, and  $\mathbf{e}$  for the angle between the  $x$  axis and the normal from the origin to the line. Let  $f(x, y)$  be a 2-dimensional function (for our purposes a gray-tone image). The mathematical definition of the Radon transform of  $f(x, y)$  for projections along straight lines writes then as:

$$R(\mathbf{r}, \mathbf{e}) = \int \int_{-\infty}^{\infty} \delta(\mathbf{r} - x \cdot \cos \mathbf{e} - y \cdot \sin \mathbf{e}) f(x, y) dx dy \tag{3}$$

The Radon transform  $R(\mathbf{r}, \mathbf{e})$  is a 2-dimensional integral transformation with the kernel  $\delta(\mathbf{r} - x \cos \mathbf{e} - y \sin \mathbf{e})$ .  $\delta$  stands for the Dirac function. All points on a Kikuchi line are transformed to one single point  $(\rho, \epsilon)$ , and a band of high intensity is transformed to a butterfly-shaped peak in Cartesian Radon space whereby the intensity is accumulated from the intensities of the individual points on the line or band, respectively. If the line or the band is fragmented, the accumulated peak intensity is reduced according to the missing sections, but all co-linear

points in the diffraction pattern are still taken into account correctly. Allowance is made for the decrease in line length with increasing distance from the center of the digitized Kikuchi pattern as well as for image artifacts by normalizing the Radon transforms on a Radon transform of a flat image of the same size. The task of locating (fragmentary) lines or bands in the diffraction pattern is thus reduced to the simpler task of locating isolated peaks in Radon spaces. The extraction of band positions is performed by peak profile analysis. The concept of the *Hough transform* [HOUGH, 1962; DUDA and HART, 1972] is similar to the Radon transform, if a *binary* rather than a *gray-tone* image is considered. A "*modified Hough transform*" in combination with special filter masks has been introduced by [KRIEGER LASSEN, 1994] for localizing Kikuchi bands in backscatter Kikuchi patterns.

The so located bands are sorted according to their intensities and widths. Indexing is based on the comparison of measured interplanar angles (which correspond to the angles between the Kikuchi bands) and interplanar spacings (which are represented by the band widths) with theoretical values in a look-up table calculated in advance for the actual crystal structure. The large angular range of backscatter Kikuchi patterns favors correct indexing. Reference directions in the specimen space (e.g., the specimen normal direction (hkl), and a direction in the specimen surface [u,v,w]) are finally indexed. The crystallographic orientation of the grain is described either in (hkl)[uvw] notation, or by three Euler angles,  $(j_1, F, j_2)$ , or by the rotation matrix,  $\mathbf{g}$ , which transform the specimen coordinate system under consideration into the crystal-fixed coordinate system.

At present 20,000 grain orientations per hour or more can be measured automatically on a chosen raster field by digital beam scan. This high speed enables the acquisition of a statistically relevant number of grain orientations in a reasonable time as well as dynamic *in-situ* experiments. Accuracy of orientation measurement with the SEM is limited to about 1° to 2°. This is often sufficient for analyzing crystal texture. A detailed study of misorientations or the distribution of special grain boundaries, however, might require a higher precision of the individual lattice orientation values. Then the transmission Kikuchi technique in the TEM [SCHWARZER, 1997b] or micro-Kossel x-ray diffraction are superior.

The maximum number of indexed bands versus the number of bands that have been considered for indexing a pattern can be used as a measure of probability that a correct solution has been found. There are various ways of defining a statistical "confidence value" or "likelihood". The confidence value is most useful in discriminating phases by ACOM [SCHWARZER et al., 2000].

The less perfect the diffracting crystal volume is, the more diffuse appears the corresponding Kikuchi pattern. The blur indicates a high density of point defects or dislocations, lattice strain, thermal lattice vibrations due to the Debye-Waller factor, micro-fragmentation of the lattice or the superposition of diffraction patterns from several grains covered at a time by the primary beam spot. A diffuse pattern may also result from a foreign surface layer such as carbon of excessive thickness (which may have been deposited by intention in order to avoid specimen charging), a contamination layer due to poor vacuum conditions or a deformation layer from inadequate sample preparation. The blur can be expressed as a quantity, named "*pattern quality*", PQ: The 1D Fourier transform of the Radon transform  $R(\mathbf{r}, \mathbf{e})$  corresponds to a 2D Fourier transform of the initial diffraction pattern  $f(x, y)$  ("*Fourier slice theorem*") [MORNEBURG, 1995]. However, the Radon transform means an integration of band intensity along the particular band. Hence noise along this direction is fairly well averaged off, and moreover, the 1D Fourier coefficients along  $\rho$  describe the averaged shape *across* the particular band. Pattern quality is therefore defined as the "sharpness" of band edges, i.e., it is measured by the magnitudes of high Fourier frequencies in band normal direction. This approach has two important advantages over a 2D Fourier transform of the initial diffraction pattern [Krieger Lassen et al., 1994]: First,

calculation of the 1D Fourier transform is significantly faster. Second, the calculated value of pattern quality is less affected by pixel noise, because the 2D approach yields Fourier coefficients as averages over *all* polar directions. Pattern quality maps of deformed, coarse-grain metals often show features which look like a dislocation network. They clearly reveal grain boundaries and surface scratches (cf. Figure 3b).

#### 4. The Microstructure Function and Graphical Representations

It is a unique feature of an analytical SEM with an ACOM facility that the determination of the microstructure function is enabled at a high spatial resolution with reasonably low effort: Scanning across the specimen surface yields two spatial coordinates  $\{x, y\}$  of the measured spot. The third dimensional coordinate  $\{z\}$  can be obtained in principle by serial sectioning. For every measured grid point  $\{x, y\}$ , the grain orientation,  $g(r)$ , as the prime objective of ACOM is readily available along with the pattern quality as a (semi-quantitative) measure of  $S(r)$ , i.e., the local dislocation density and lattice strain. *Phase discrimination* can be done at the same time by checking possible crystal lattices for consistent indexing, provided that the lattice parameters and crystal structures of the phases are sufficiently different. Additional information about the local elemental composition, e.g., from a simultaneous EDS analysis, may be helpful to rule out less likely phases in advance. *Phase identification* without *a priori* knowledge of possible phases has been carried out by using a scientific grade slow-scan cooled CCD camera for the acquisition of high quality backscatter Kikuchi patterns [Michael and Goehner, 1993]. Phases of selected areas have then been determined by comparing the volume of the elementary lattice cell calculated from the indexed Kikuchi pattern with values in the international tables of crystallography.

Crystal lattice orientation measurement grain by grain yields information on the microstructure which is not obtained by any other technique. In particular the study of correlations between spatial and orientation parameters is enabled. The spatial distributions of lattice orientations in the surface of a bulk polycrystal or in a polycrystalline thin foil may be illustrated graphically by the construction of pseudo-color maps of the microstructure (Crystal Orientation Maps = COM) whereby grains of a specific orientation are stained by a specific color [GERTH and SCHWARZER, 1993]. Pseudo-colors can be defined for the grain orientations by overlaying a color triangle on two standard triangles, one for the  $\{hkl\}$  and one for  $\langle uvw \rangle$  reference directions, or by attributing the three basic colors to the three Euler angles,  $\{\varphi_1, \mathbf{F}, \mathbf{j}_2\}$ , or to the three parameters of the Rodrigues vector,  $\mathbf{R} = \mathbf{n} \cdot \tan(\omega/2)$ . In a similar way, misorientations  $\Delta g$  across grain boundaries,  $\Sigma$  values of "special" grain boundaries, or other microstructural characteristics such as dislocation densities, activated glide systems, types of twins, the Schmid factor, or resolved shear stress are visualized [SCHWARZER, 1997b]. ACOM will enable a major advance in stereological evaluation of the microstructure. A grain is simply defined by a contiguous array of points of uniform orientation. The number fractions of measured points with one or several properties under consideration can so directly be equated to area fractions, e.g., to evaluate the statistical grain size distribution, the grain size distribution as a function of preferred orientations, misorientation frequency as a function of grain size, the distribution of "special" grain boundaries by number and length, phase distributions, and many more.

#### 5. Examples of Applications

##### 5a. Microstructure and texture in metal interconnects

Thin films, deposited on a solid substrate by electroplating, by sputtering or by evaporation under high vacuum, often exhibit a marked fiber texture. It is well established that

electromigration failure in aluminum interconnect lines is closely related to their microstructure, i.e., the texture, grain size and dislocations [KNORR and SZPUNAR, 1994; HU, 1995]. The aluminum circuits on SiO<sub>2</sub>/Si substrates have been patterned in continuous metallization layers by standard photolithography and subtractive chemical etching or subtractive reactive ion etching processes. A microstructure consisting of uniformly sized "bamboo" grains, i.e. the line width is much smaller than the mean grain size, proved to be a key to good performance. The main diffusion paths in electro-migration are supposed to be grain boundaries and interfaces where - at moderate temperatures - diffusion is faster than through the lattice. In these layers the grains have a columnar shape whereby, in case of a sharp fiber texture, the majority of grain boundaries are pure tilt boundaries. The axes of tilt are parallel with the fiber axis. The tilt grain boundaries can be described by an array of edge dislocations which are orientated perpendicular to the layer plane and the electron flux. Without dislocation overlap, they do not provide long-range diffusion paths for electromigration. In a well developed fiber texture, any angle of lattice tilt is possible between abutting grains, unless preferred misorientations are imposed either by the deposition process or by some epitaxial growth from the substrate. Triple points, however, cause flux divergence along the grain boundaries and are hence a geometrical source of electromigration failure. Another detrimental geometry are "blocking" grains with a grain boundary that cuts the interconnect line perpendicular to the flux direction.

In addition to the shape and geometrical arrangement of the grains, individual lattice orientations turn out to have a major effect on the formation of hillocks and voids by electromigration. Grains deviating from the common  $\langle 111 \rangle$  fiber texture supply grain boundaries with a twist component which might increase grain boundary diffusion. They are candidates for thermomechanical hillock growth during thermal cycling and electromigration, as has been shown by measuring the lattice orientations of individual hillocks and their neighbors [GERTH et al., 1994a]. This behavior has been explained by the following working hypothesis [SCHWARZER, 1997c]: Due to the large thermal mismatch of the metallization layer and the silicon substrate, a biaxial mechanical strain/stress is caused at every temperature jump. Grains deviating from the common fiber texture are softer, since they have a significantly higher Schmid factor than the  $\langle 111 \rangle$  orientated grains with respect to the biaxial stress field. They can be deformed by preference, and thermomechanical stress is relaxed during heating cycles by material transport from the harder grains of  $\langle 111 \rangle$  fiber orientation. At extremely high current densities, the "electron wind" will superimpose a further preferred direction on diffusion. This effect is known as electrodiffusion or electromigration. During cooling cycles, however, diffusion is intercepted due to a lower temperature, and the mass transport is not reversed. High local stress is then relaxed by glide processes rather than diffusion. On the whole, mass depletion and grain collapse takes place at the harder grains, while mass is accumulated during thermal cycling at locations with orientations far away from the common  $\langle 111 \rangle$  fiber texture, i.e. hillocks are formed. The final confirmation of this hypothesis requires the measurement of local stress in addition to grain orientation on a mesoscale.

Stress-induced grain growth of the aluminum metallization layer by thermal cycling is not recommended before patterning the interconnect structure. Although large uniform grain sizes can thus be produced for a "bamboo" microstructure of the interconnects, but the sharp initial  $\langle 111 \rangle$  fiber texture is distinctly weakened at the same time. Increasingly more "soft" grains with large deviations from the favorable  $\langle 111 \rangle$  fiber texture are formed [GERTH et al., 1994b].

To overcome the unsolved problems of electromigration failure in aluminum interconnects, copper is now considered a leading candidate for metallization of advanced integrated circuits. The damascene process has almost entirely replaced the former direct etching process developed for aluminum patterning. In the first step, the line pattern is

formed by producing well-defined trenches with smooth walls in the  $\text{SiO}_2/\text{Si}$  substrate. Reliable processes of silicon photolithography and reactive ion etching are employed. Then a diffusion barrier, a dielectric layer and a copper seed layer are sputter deposited. The next step is the deposition of a thick continuous copper layer by electroplating. Finally, the excess metal is removed by chemical-mechanical polishing down to the substrate surface. The trenches, now filled with copper, remain to serve as the interconnect lines.

In the case of damascene architecture, the simultaneous growth of some copper grains from the bottom and others from the sidewalls of the trench will lead to non-columnar grain shapes and to double fiber textures. The consistent control of grain orientation in the metallization layers is therefore critical for process optimization. Figure 2 shows the crystal orientation map of five parallel damascene copper interconnect lines [HUOT et al., 1999]. The trenches were  $1\ \mu\text{m}$  wide and  $0.5\ \mu\text{m}$  deep. A 50 nm tantalum layer had been deposited as a barrier to protect the silicon semiconductor from diffused copper. After the electroplating process the wafers were annealed for 10 min. at  $120\ ^\circ\text{C}$ . Finally the continuous copper layer was removed down to the substrate. No top layers have been deposited on the batch, because they might be an obstacle to ACOM measurement. The individual grains are clearly distinguished from each other by orientation-specific pseudo-colors (respectively gray shades in the print). It is worth mentioning that individual grains are hardly recognized in SEM micrographs, in contrast to crystal orientation maps and FIB micrographs, since orientation contrast is low, and there is no grooving of the grain boundaries seen.

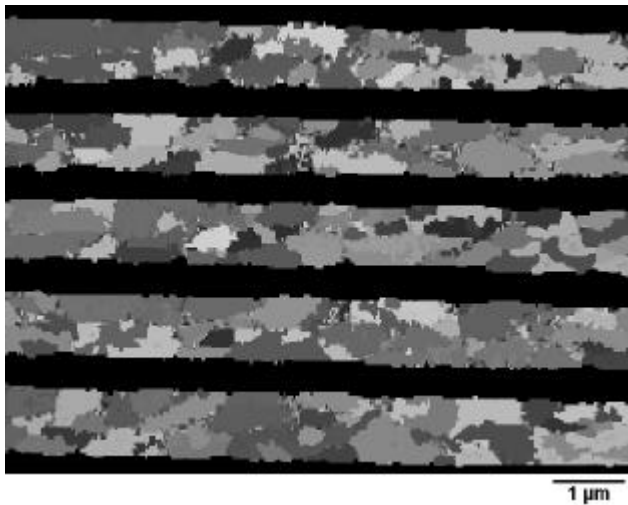


Fig. 2: Crystal orientation map of electroplated copper interconnect lines produced by the damascene process.

A fragmented central seam of grain boundaries has been formed in the interconnect lines (Figure 2). It indicates simultaneous growth of copper grains from the bottom and from the sidewalls of the trenches. The unwanted seam may form a path of increased diffusion leading to decreased electromigration resistance. Competing grain growth in two directions may also produce a variety of general grain boundaries. By additives to the electrolytic bath and appropriate electroplating conditions, crystal growth from the sidewalls can be suppressed in favor of grain growth from the bottom. Seamless interconnect lines are then obtained.

The mutual arrangement and shape of the grains in Figure 2 have been used to distinguish the grains of competing growth directions [HUOT et al., 1999]. The orientation distribution function (ODF) and pole figures have been calculated from the individual grain orientations separately for those grains which fill an interconnect line at full width ("bamboo" grains) and

for those grains which form a central seam. For both types of grain, a strong  $\langle 111 \rangle$  and a weak  $\langle 511 \rangle$  fiber texture have been found which are aligned either in the specimen normal direction, i.e. for grains growing from the bottom of the trenches, or normal to the sidewalls of the trenches, according to this growth direction. It is clearly shown that the geometry of the trenches has imposed strong constraints on the development of microstructure and on texture.

### 5b. Changes in microstructure by plastic deformation

ACOM offers a powerful technique for revealing changes of microstructure and inhomogeneous distributions of crystal texture caused by plastic deformation. A Swedish 5 Öre coin may serve as an example. Before ACOM measurement was carried out, the coin surface has been ground and electropolished by standard metallographic techniques to a flat such that the coinage pattern was no longer visible.

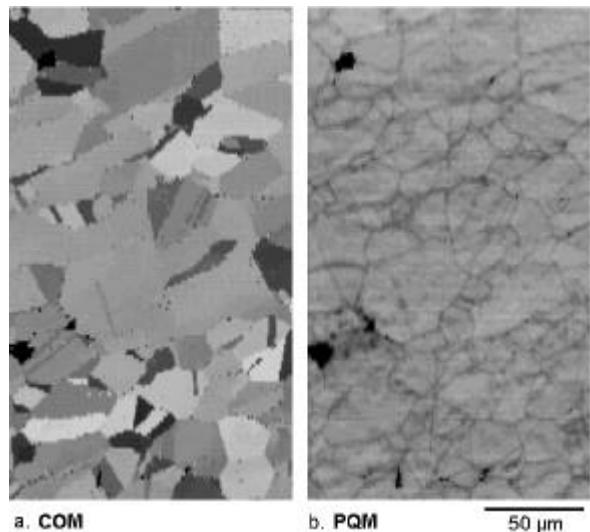


Fig. 3: (a) Crystal Orientation Map and (b) Pattern Quality Map of a section of a polished Swedish 5 Öre coin. (65,000 measured orientation points.)

Figure 3 shows a small section of the coin with one dot of the "Ö"re inscription. The chased grooves of the minting stamp caused a heavy flow of the material. At the slopes of the dot, plastic deformation results in a small grain size and formation of twins. Therefore, the dot can be perceived again in the crystal orientation map of the flat surface in the form of a ring of small grains. The central part of the dot and the embossed flat regions of the minting stamp produced a more homogeneous compression of the coin material in normal direction to the surface. Here, deformation was obviously low enough to maintain the microstructure of the initial rolled sheet metal. When approaching a grain boundary, the beam spot is falling on both grains, two Kikuchi patterns are overlaid, and as a consequence indexation fails in a few cases. These points are marked black. The pattern quality map (Figure 3b) clearly reveals the grain boundaries as sites of reduced crystallographic perfection. It is worth noting that the pattern quality value, calculated from the 1D Radon transform of the Kikuchi pattern, is only marginally affected by the mere superposition of patterns.

### Acknowledgment

Financial support by the German Research Foundation (DFG project SCHW 403/7-1 "Elektromigration") is gratefully acknowledged. The authors would like to thank Dr. A.H. Fischer, Infineon Technologies Munich, for providing the damascene copper interconnect specimen.

## References

- ADAMS, B.L., WRIGHT, S.I., KUNZE, K.: Metallurgical Transactions 24A (1993) 819.
- ALAM, M.N., BLACKMAN, M., PASHLEY, D.W.: Proc. Roy. Soc. 221 (1954) 224.
- BETHGE, H., HEYDENREICH, J. (eds.): Elektronenmikroskopie in der Festkörperphysik, VEB Verlag Deutscher Wissenschaften, Berlin 1980.
- BUNGE, H.J.: Grain Orientation and Texture. In: Industrial Applications of X-Ray Diffraction, Eds. F.H. Chung and D.K. Smith, Marcel Dekker, New York, Basel 2000.
- BUNGE, H.J., SCHWARZER, R.A.: Advanced Engineering Materials (March 2001)
- BRÜMMER, O., STEPHANIK, H. (eds.): Dynamische Interferenztheorie: Grundlagen und Anwendungen bei Röntgenstrahlung, Elektronen und Neutronen. Akademische Verlagsges., Leipzig 1976.
- BRÜMMER, O., HEYDENREICH, J., KREBS, K.H., SCHNEIDER, H.G.: Handbuch Festkörperanalyse mit Elektronen, Ionen und Röntgenstrahlen, Vieweg Braunschweig/Wiesbaden 1980.
- DEANS, S.R.: The Radon Transform and Some of Its Applications, John Wiley & Sons Inc., New York 1983.
- DUDA, R.O., HART, P.E.: Comm. ACM 15 (1972) 11.
- FISCHER, A.H., SCHWARZER, R.A.: Materials Science Forum vol. 273-275 (1998) 673.
- GERTH, D., SCHWARZER, R.A.: Textures and Microstructures 21 (1993) 177.
- GERTH, D., KATZER, D., SCHWARZER, R.A.: phys. stat. sol. (a) 146 (1994a) 299.
- GERTH, D., ZAEFFERER, S., SCHWARZER, R.A.: Materials Science Forum vol. 157-162 (1994b) 1205.
- HOUGH, P.V.C.: Methods and means for recognizing complex patterns. US patent 3069654, 1962.
- HU, C.-K.: Thin Solid Films 260 (1995) 124.
- HUOT, A., FISCHER, A.H., VON GLASOW, A., SCHWARZER, R.A.: Quantitative Texture Analysis of Cu Damascene Interconnects. In Eds.: O. Kraft, E. Arzt, C.A. Volkert, P.S. Ho, and H. Okabayashi: Stress induced phenomena in metallization. AIP Conf. Proc. 491, Melville, New York 1999.
- KNORR, D.B., SZPUNAR, J.A.: Journal of Materials 46 (1994) 42.
- KRIEGER LASSEN, N.C.: Automated Determination of Crystal Orientations from Electron Backscattering Patterns, Ph.D. Thesis, Danmarks Tekniske Universitet, Lyngby, 1994.
- KRIEGER LASSEN, N.C., JUUL JENSEN, D., CONRADSEN, C.: Materials Science Forum vol. 157-162, Part 1 (1994) 149.
- MICHAEL, J.R., GOEHNER, R.P.: MSA Bulletin 23 (1993) 168.
- MORNEBURG, H.: Bildgebende Systeme für die medizinische Diagnostik, Siemens & Publicis MCD Verlag, Munich 1995.
- NISHIKAWA, SH., KIKUCHI, S.: Proc. Imp. Acad. Japan 4 (1928) 475.
- RADON, J.: Ber. Verh. Sächs. Akad. Wiss. Leipzig, Math.-Naturw. Klasse 69 (1917) 262.
- REIMER, L.: Transmission Electron Microscopy, Springer-Verlag, Berlin 1984.
- SCHÄFER, B., SCHWARZER, R.A.: Materials Science Forum vol. 273-275 (1998) 223.
- SCHWARZER, R.A.: Micron 28 (1997a) 249.
- SCHWARZER, R.A.: Ultramicroscopy 67 (1997b) 19.
- SCHWARZER, R.A.: Mat. Res. Symp. Proc. Vol. 472 (1997c) 281- 292, Pittsburgh/PA.
- SCHWARZER, R.A., SUKKAU, J.: Materials Science Forum vol. 273-275 (1998) 215.
- SCHWARZER, R.A., SINGH, A.K., SUKKAU, J.: Materials Science and Technology (2000) *in press*.

### Contact information:

Prof. Dr. Robert SCHWARZER\*  
 Dipl.-Ing. Agnès HUOT  
 Physikalisches Institut der TU, AG Textur  
 Leibnizstr. 4  
 38678 Clausthal-Zellerfeld

\*corresponding author  
 Email: schwarzer@tu-clausthal.de